Journal of Materials Chemistry

Cite this: J. Mater. Chem., 2012, 22, 23921

www.rsc.org/materials

PAPER

Significant electrochemical stability of manganese dioxide/polyaniline coaxial nanowires by self-terminated double surfactant polymerization for pseudocapacitor electrode†

Afriyanti Sumboja, Ce Yao Foo, Jian Yan, Chaoyi Yan, Raju Kumar Gupta and Pooi See Lee*

Received 19th April 2012, Accepted 2nd October 2012
DOI: 10.1039/c2jm32456c

Manganese dioxide/polyaniline coaxial nanowire networks are prepared by using double surfactant approach. This approach improves the interaction between the two active materials which has been confirmed by FTIR and XPS measurements, and yields a controllable uniform thin coating of polyaniline on the well-dispersed manganese dioxide nanowires. This hybrid heteronanostructure enhances the conductivity and capacitive performance of the supercapacitor electrode. The electrochemical test delivers specific capacitance as high as 498 and 873 F g^{-1} at 2 and 0.25 A g^{-1}, respectively. Good cycling stability of up to 5000 cycles (5% capacitive degradation) outperforms other currently available redox nanocomposite electrodes. This result shows that the interaction among the active materials and improved nanostructure design are the two important factors to boost up the electrochemical performance of the hybrid nanomaterials. This work illustrates a promising platform that can be adopted for a myriad of metal oxide-conducting polymer nanocomposites while reaping the benefit as low cost electrode material for supercapacitor application.

1. Introduction

Supercapacitor or electrochemical capacitor has been considered as promising energy storage for hybrid electric vehicle and other portable devices due to its ability to combine fast power delivery of conventional capacitor and high energy storage of battery. It can be classified according to its charge storage mechanism and active materials used. EDLC or electrical double layer capacitor stores charges by reversible ions adsorption onto high surface area of active materials, such as carbonaceous based materials. Recently, more attention has been developed on the pseudocapacitor which in many cases can exceed the performance of EDLC due to the presence of fast and reversible faradaic charge storage process.[1] Transition metal oxides and conducting polymers have been identified to exhibit such pseudocapacitive behavior.[1,2]

Among the transition metal oxides, manganese dioxide (MnO_2) has gained considerable attention as an alternative electrode material due to its low cost, wide abundance, and environmental friendliness.[3,4] Most of the reports on MnO_2 based supercapacitor have been focusing on improving its specific capacitance through nanostructuring method.[4–9] However, relying on the nanostructuring of single electrode materials may not always yield an optimum supercapacitive performance of the electrode material, as some of the intrinsic properties of the materials cannot be simply altered by nanostructuring. For example, the poor electronic conductivity of MnO_2 (10^{-5} to 10^{-6} S cm^{-1})[10] often results in the high internal resistance of the electrode and low power density of the device. On the other hand, polyaniline (PANI) is one of the most studied conducting polymers due to its high doping level, good electrical conductivity and environmental stability. Theoretically, specific capacitance (C_{sp}) of PANI is able to reach 2000 F g^{-1}.[11] However, due to the variation on its synthetic routes and morphologies, C_{sp} of PANI is found to vary between 160 and 815 F g^{-1}.[12] Thin PANI coating has to be maintained in order to facilitate the electrolyte ions to reach all the active materials.[13,14]

Combining two or more electrode materials to form heterostructured nanomaterials has attracted significant attention as they do not only improve the performance through the effect of the size confinement, but also with the added functionalities or synergistic properties.[1] By integrating different active materials and tailoring the properties of each material, we are able to exploit their potential as high performance electrodes. Heterostructured nanomaterials have been constructed with various configurations,[15,16] highlighting the importance of architecturing

School of Materials Science and Engineering Nanyang Technological University, 50 Nanyang Avenue, 639798, Singapore. E-mail: pslee@ntu.edu.sg; Fax: +65 6790 9081; Tel: +65 6790 6661

† Electronic supplementary information (ESI) available: TEM images of MnO_2/PANI coaxial NW synthesized at different MnO_2 loading, HCl and aniline concentration. Mn 2p XPS core level spectra of MnO_2/PANI coaxial NW. Charge discharge curves of MnO_2 NW, MnO_2/PANI coaxial NW and PANI at different applied currents. Cyclic voltammograms of MnO_2 NW, MnO_2/PANI coaxial NW and PANI at 50 mV s^{-1}. Literature data on MnO_2/PANI based electrodes for supercapacitor application and calculation method. See DOI: 10.1039/c2jm32456c

suitable structure for ideal electrode of electrochemical energy storage. One of the strategies is to use coaxial nanowires, in which the core materials are mainly used to store the charges while the shell is particularly responsible for the electrochemical stability and conductivity of the sample.[15] Alternatively, the core can be a good conductor which acts as a continuous pathway for kinetics process whereas the active materials are coated on it.[8]

Heterostructured hybrid nanomaterials which consist of transition metal oxide and conductive polymer have been reported sporadically. This combination has the potential to exhibit excellent properties for capacitive performance due to the dual charge storage redox processes contributed from both materials. MnO_2 compositing with poly(3,4-ethylenedioxythiophene), polypyrrole or PANI showed moderate to high specific capacitance (300–700 F g^{-1}). However, their cycling performances are still far from satisfactory. The typical cycling test results show tens of percentage degradation within relatively short cycling test.[17–29] Poor long term cycling stability of the hybrid redox nanomaterials has not been addressed by most of the reports and it is currently one of their major drawbacks that prevent their application in real device. Li *et al.* have prepared MnO_2 and PANI as shell materials on CNT network to form the ternary coaxial nanostructures. C_{sp} of 330 F g^{-1} has been achieved with 23% degradation of C_{sp} after 1000 cycles.[27] Recently, Jaidev *et al.* have reported PANI and manganese oxide hybrid which showed good C_{sp} (626 F g^{-1}) but poor cycling stability, 33% degradation of C_{sp} after 1000 cycles.[28] Composite structure prepared by electrodeposition of both redox materials tends to have high C_{sp}. Zhou *et al.* have deposited manganese oxide and PANI on porous carbon and achieved 500 F g^{-1} with 40% degradation of C_{sp} after 5000 cycles.[25] Sun and Liu have reported fibrous structure of MnO_2 and PANI deposited on carbon cloth with C_{sp} of 532 F g^{-1} and 24% capacitive degradation after 1200 cycles.[23] Prasad and Miura have deposited MnO_2 and PANI on stainless steel and were able to achieve 715 F g^{-1} with 3.5% degradation after 5000 cycles.[30] Liu and Lee have coelectrodeposited MnO_2 and poly(3,4-ethylenedioxithiophene) coaxial nanowires with the capacitance up to 210 F g^{-1}.[31] Although electrodeposited film has great potential especially in micro-scale devices, powders of active materials are necessary in most of the applications for the ease of further processing and versatile choice of current collectors.[18]

One of the problems in the metal oxide/conducting polymer heterostructures is the weak interaction between these two materials, thus it limits the optimum capacitive properties of the nanocomposite.[19] Hence, feasible strategies to enhance the interaction between the heterogeneous components are required. One such approach would be the controlled polymerization of the conducting polymer onto the surface of the metal oxide using an electrostatically bonded double surfactant layer assisted polymerization method. This method has been first introduced by Zhu *et al.* to produce hollow PANI capsules from metal oxides micro sized particles as the sacrificial template. The key mechanism of this method is to slow down and control the polymerization on the substrate materials rather than in the solution.[32] In this communication, instead of using micron sized metal oxides particles as sacrificial templates, we employed MnO_2 nanowires as the core material and a PANI layer was polymerized onto the MnO_2 nanowires by using the modified double surfactant method to form the MnO_2/PANI coaxial nanowires network. We reveal that the presence of electrostatically bonded surfactants has enhanced the doping and conductivity level of PANI as well as the capacitive performance.

Besides serving as an electroactive material for the energy storage process, PANI also acts as a coating layer which ameliorates MnO_2 from dissolution into electrolytes.[26] A conductive polymer coating has also been shown to minimize dissolution of polysulfides in Li-sulfur batteries, improving their long term stability.[33] In addition, the entanglement of PANI chains will be prevented by the addition of MnO_2 nanoparticles due to the electrostatic repulsion between positively charged MnO_2 in the acidic co-polymerization media.[19] The nano-scaled structure of PANI serves to enhance the active surface area and improves the ions accessibility onto the electrochemically active surfaces. Therefore, improvement on the electronic conductivity, specific capacitance and cycling stability can be achieved from this heterostructured electrode.

2. Experimental

2.1. Synthesis of the materials

MnO_2 nanowires (MnO_2 NW) were synthesized according to our previous report.[34] In brief, $Mn(NO_3)_2$ (13.8 mL, 0.1 M) was added into the solution and quickly followed by $KMnO_4$ (20 mL, 0.1 M). The solution was transferred into autoclave for hydrothermal process and heated at 150 °C for 6 hours. The black precipitate was centrifuged and washed with deionized water for several times. Then, precipitates were dried at 65 °C.

MnO_2/PANI coaxial NW were synthesized using a modified double surfactant method.[32] In brief, 5 g of polyvinylpyrrolidone (PVP) and 0.05 g of MnO_2 nanowires were weighed and mixed into a centrifuge tube containing 60 mL of DI water. The content was sonicated for 8 hours. After which, they were centrifuged for several times in ethanol. 0.08 g of sodium dodecyl sulfate (SDS) and 0.05 g of ammonium persulfate (APS) were then dissolved in 50 g DI water. The remaining content from the centrifuge tube was transferred into SDS and APS solution and aged at room temperature for 12 hours. 0.008 mL of aniline monomer and 15 mL of 0.1 M HCl were added into the solution. It was then stirred continuously in an ice bath (4 °C) for 8 hours and centrifuged in ethanol before drying the product overnight.

PANI powders were synthesized using a similar method with MnO_2/PANI coaxial NW without the addition of PVP modified MnO_2. In brief, 0.08 g of SDS and 0.05 g of APS were prepared in 50 g DI water. Then, 0.008 mL of aniline monomer and 15 mL of 0.1 M HCl were added into the solution. It was then stirred continuously in an ice bath (4 °C) for 8 hours and centrifuged in ethanol before drying the product overnight.

2.2. Materials and electrochemical characterization

The morphology and microstructure of the powder were investigated using scanning electron microscopy (SEM, JEOL-7600F) operated at 5 kV and transmission electron microscopy (TEM, JEOL 2010) operated at 200 kV. TEM energy dispersive X-ray spectroscopy was used to perform the elemental analysis of the sample (TEM, JEOL 2010F). Crystal structure of the synthesized powder was studied by powder X-ray diffractometer (Bruker D8

Advance) with Cu Kα radiation (1.5506 Å) at room temperature. The diffractometer was operated at voltage of 40 kV and current of 40 mA. Fourier transform infrared spectra were measured by Perkin Elmer Fourier transform infrared spectroscopy (FTIR) system by making pellets with KBr powder. The FTIR resolution was set at 0.5 cm^{-1} with scan number of 30. X-ray photoelectron spectroscopy (XPS) analysis was carried out on a Kratos Analytical AXIS HSi spectrometer with a monochromatized Al Kα X-ray source (1486.6 eV) at a constant dwell time of 100 ms and a pass-energy of 40 eV. The X-ray source was run at a reduced power of 150 W. The pressure in the analysis chamber was maintained at 7.5×10^{-9} Torr or lower during each measurement. All binding energies were referenced to the C 1s hydrocarbon peak at 284.6 eV.

Quantitative analyses of MnO_2 and MnO_2/PANI were carried out as follows. 0.1 mg of the as synthesized MnO_2 NW and MnO_2/PANI coaxial NW samples were dissolved respectively in 6 M HNO_3 (10 mL) through continuous ultrasonication for several hours. They were then diluted 10-fold with DI water. Concentration of Mn in both solutions was measured by using inductively coupled plasma mass spectrometry ICP-MS (Perkin Elmer Elan DRC-e) by further diluting the solutions 10-fold.

Working electrode materials were prepared by mixing the as synthesized powder (85 wt%), carbon black (10 wt%), and poly(vinylidene fluoride) (PVDF) (5 wt%). A few drops of *N*-methylpyrrolidinone (NMP) were added to form slurry. It was then coated on the carbon paper and dried under vacuum at 65 °C for 8 hours. The mass of each electrode was about 0.2 ± 0.02 mg cm^{-2}. Electrochemical studies were carried out by using Solartron, 1470E electrochemical interface. Three electrodes set up in Na_2SO_4 (1 M) electrolyte were used, with platinum sheet and saturated Ag/AgCl as a counter and reference electrode respectively. Electrochemical impedance spectroscopy (EIS) measurements were conducted on constant voltage mode by sweeping the frequency from 55 kHz to 20 mHz at amplitude of 5 mV.

3. Results and discussion

The key for uniform and thin polymer coating on the metal oxide is to control the rate of polymerization, so that we can prevent the excessive polymerization on the surface or in the bulk solution. The schematic illustration of the typical synthesis process of MnO_2/PANI coaxial nanowires using double surfactant assisted polymerization method is shown in Scheme 1. Polar amide of PVP molecule is first adsorbed onto the MnO_2 NW during the sonication process. When the MnO_2 modified PVP is dispersed into the SDS solution, the SDS molecules form the second layer of surfactant with the negative side of the SDS molecules facing outwards in the solution. The anilinium ions (An^+) are then adsorbed onto the surface of MnO_2 NW due to the static interaction. Thus, the polymerization prefers to take place on the surfaces of MnO_2 NW. In addition, as the concentration of aniline monomer in the solution is low, the polymerization process is initiated and self terminated on the surface of MnO_2 only, resulting on the uniform coating of PANI on MnO_2 NW.[32]

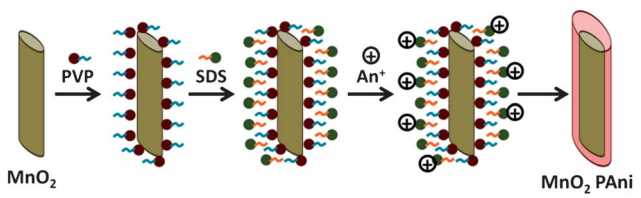

Scheme 1 Schematic synthetic route for preparation MnO_2/PANI coaxial nanowires structure.

The morphology of MnO_2 NW and MnO_2/PANI coaxial NW samples as imaged using SEM and TEM are shown in Fig. 1. MnO_2 samples synthesized using hydrothermal treatment at 150 °C displayed nanowires features with diameter about 75 nm (Fig. 1a and d). Uniform coating of PANI has been observed upon polymerization of PANI using double surfactant assisted polymerization method on the MnO_2 NW, forming MnO_2/PANI coaxial NW (Fig. 1b). The overall homogeneous coating of PANI is shown in the TEM image in Fig. 1e, with some parts of the nanoscaled PANI forming irregular minor protrusions from the PANI surface. TEM-EDS of MnO_2/PANI coaxial NW is shown in Fig. 1f. Besides C, N, and O, Mn signal is also detected in the EDS spectrum which confirms the presence of MnO_2 in our sample. In addition, S peak is also observed and originated from SDS and APS that were used during the synthesis. The presence of Cu peak is due to Cu grid used during TEM analysis, while weak K peak came from $KMnO_4$ residue in the sample.

Different concentration of HCl used during the double surfactant assisted polymerization has shown to affect the thickness of the PANI coating. PANI could not be found on the MnO_2 NW at low concentration of HCl (10^{-3} to 10^{-2} M). At higher concentration of HCl (0.1 M), uniform coating of PANI was observed on the MnO_2 NW and with an estimated thickness of 30 nm. The thickness of PANI coating can be adjusted by varying the monomer concentration of aniline as well as the amount of acid and MnO_2 added during the polymerization process (ESI Fig. S1†). We have also prepared a PANI sample synthesized using the same method without adding PVP modified MnO_2. As synthesized PANI powder shows big flakes morphology (Fig. 1c).

XRD and FTIR measurements were used to further characterize the samples. The XRD patterns of both MnO_2 NW and MnO_2/PANI coaxial NW are shown in Fig. 2a. XRD pattern of

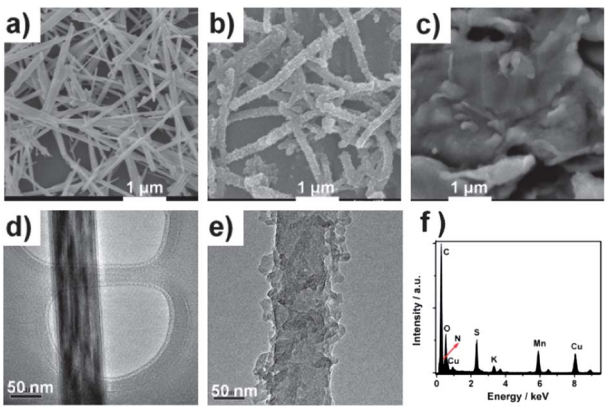

Fig. 1 (a–c) SEM image of MnO_2 NW, MnO_2/PANI coaxial NW and PANI; (d and e) TEM image of MnO_2 NW and MnO_2/PANI coaxial NW; (f) TEM-EDS analysis of MnO_2/PANI coaxial NW.

MnO_2 NW can be indexed as tetragonal hydrated α MnO_2 (JCPDS 44-0140) which is agreeable to our previous report.[34] The presence of large 1D tunnel structure (4.6 × 4.6 Å) in the α MnO_2 as a result of the edge sharing of MnO_6 octahedra enables the facile access for ions to move in and out during the charge storage process.[35] Therefore, it is well suited for supercapacitor application. XRD pattern of MnO_2/PANI coaxial NW sample shows two broad peaks at 2 theta ≈ 20° and 25° which represent the periodicities parallel (100) and perpendicular (110) to the PANI chain respectively, indicating good crystallinity of the PANI shell.[32,36] Peaks of MnO_2 NW were hardly detected from the XRD pattern of the MnO_2/PANI coaxial NW which is also observed by other works.[28,37] Gemeay *et al.* suggested that distortion of crystal structure of MnO_2 occurred during the polymerization of PANI, thus led to the formation of amorphous MnO_2.[37] The XRD peak broadening at 2 theta = 25° supports this phenomenon and it is similar to the observation reported by Jaidev *et al.*[28]

Successful PANI coating on MnO_2 NW is also confirmed by FTIR (Fig. 2b). For comparison, we have also prepared physically mixed MnO_2 NW and PANI powder. There was a strong peak observed at 1385 cm^{-1} in the spectrum of MnO_2 NW due to the stretching of OH group combined with Mn atom.[19] This IR band was also observed in the physically mixed MnO_2 PANI as well as in the MnO_2/PANI coaxial NW synthesized by double surfactant approach. Upon addition of PANI, the intensity of this peak decreased and there were additional peaks observed in the FTIR spectrum. For PANI sample, characteristic peaks due to C–N stretching vibration with aromatic conjugation were observed at 1294 and 1237 cm^{-1}. IR band at region 1120 cm^{-1} region indicates the electron delocalization in PANI and stretching of N=Q=N (Q is quinoid ring). IR bands due to the stretching vibration of quinoid and benzenoid ring were seen at 1564 and 1479 cm^{-1}, indicating that the resultant PANI was in its emeraldine state, rather than leucoemeraldine or permigraniline state.[38,39] The as-prepared MnO_2/PANI coaxial NW have identical PANI characteristic peaks as PANI powder and physically mixed MnO_2 PANI. However, the peaks in MnO_2/PANI coaxial NW were observed to be shifted to the higher wavenumber. For example, characteristic peak due to quinoid rings which was observed at 1564 cm^{-1} for both PANI powder and physically mixed MnO_2 PANI was shifted significantly to 1580 cm^{-1} in MnO_2/PANI coaxial NW. This blue shift indicates that considerable interaction exists between MnO_2 and PANI through the electrostatic PVP SDS surfactant layers.[40] The interaction between metal oxides and PANI has also been found earlier to increase the doping level and conductivity improvement of PANI,[41,42] which may be particularly useful for its electrochemical properties.

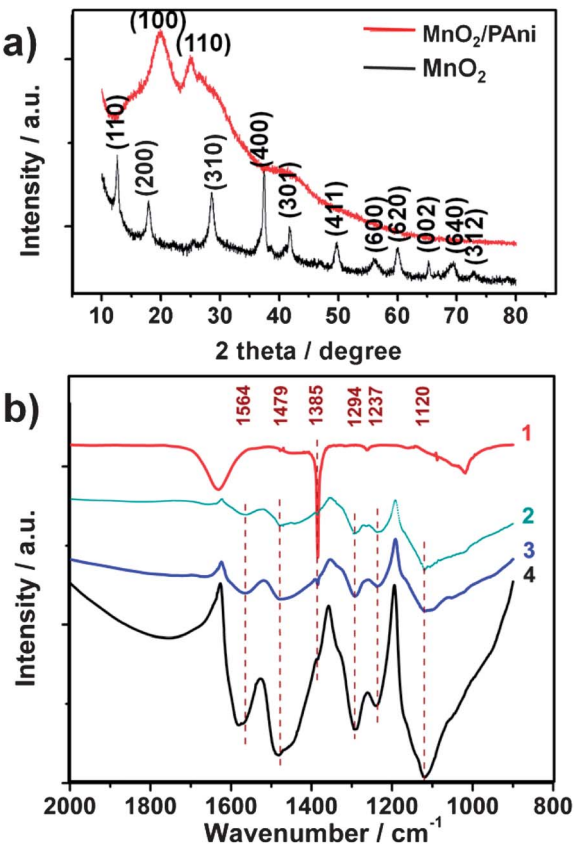

Fig. 2 (a) XRD pattern for MnO_2/PANI coaxial NW and MnO_2 NW; (b) FTIR spectrum for MnO_2 NW (1), PANI (2), physically mixed MnO_2 and PANI (3) and MnO_2/PANI coaxial NW (4).

Further characterization was performed by XPS measurements. Fig. 3a–c represent the XPS spectra of MnO_2 NW after adding PVP and SDS. Mn 2p spectral region in Fig. 3a consists of two peaks centered at 641.7 and 653.3 eV which correspond to the spin orbit doublet of Mn $2p_{3/2}$ and Mn $2p_{1/2}$, respectively.[17] Fig. 3b shows the N 1s core level spectra of PVP and SDS modified MnO_2 NW. N 1s peak can be deconvoluted into two peaks at 400 and 401.9 eV. The presence of a smaller peak at 401.9 eV confirms that some N has been transformed into protonated nitrogen species (N^+) upon aging PVP modified MnO_2 in SDS solution which indicates the cationic nature of N atom in the pyrrolidone ring of PVP.[43,44] The protonated nitrogen (N^+) helps in attaching anionic SDS molecules to PVP. The presence of SDS is confirmed through the occurrence of S 2p signal from the sample. Two peaks at 168.3 and 169.5 eV indicate the presence of sulfur atoms of the dodecyl sulfate anions, signifying the presence of SDS in the sample.[45]

Fig. 3d shows the peak of N 1s core level of PVP and SDS modified MnO_2 after polymerization of aniline. In contrast to the N 1s signal before the polymerization, N 1s signal can be deconvoluted into four peaks. The benzenoid amine is centered at 399.4 eV. The peaks at 400.8 and 402.6 eV correspond to positively charged nitrogen, which can be interpreted as polaron and bipolaron states, respectively. While the weak signal at 404.4 eV can be related to the N 1s shake up satellite of the ionized nitrogen atoms in the PANI molecular chain.[46] The presence of nitrogen cationic radical at peaks higher than 400 eV is related to the doping level of PANI which can be calculated from the ratio of the positively charged nitrogen to the total nitrogen ($[N^+]/[N]$). MnO_2/PANI coaxial NW sample shows the doping level of 0.43, indicating the good doping level of PANI which further supports our FTIR results.[13] This finding is in coherence to the doping level increment found in the reported PANI intercalated MnO_2 layered structure.[40]

The presence of MnO_2 in MnO_2/PANI coaxial NW is confirmed by XPS characterization (ESI Fig. S2†). The peaks of

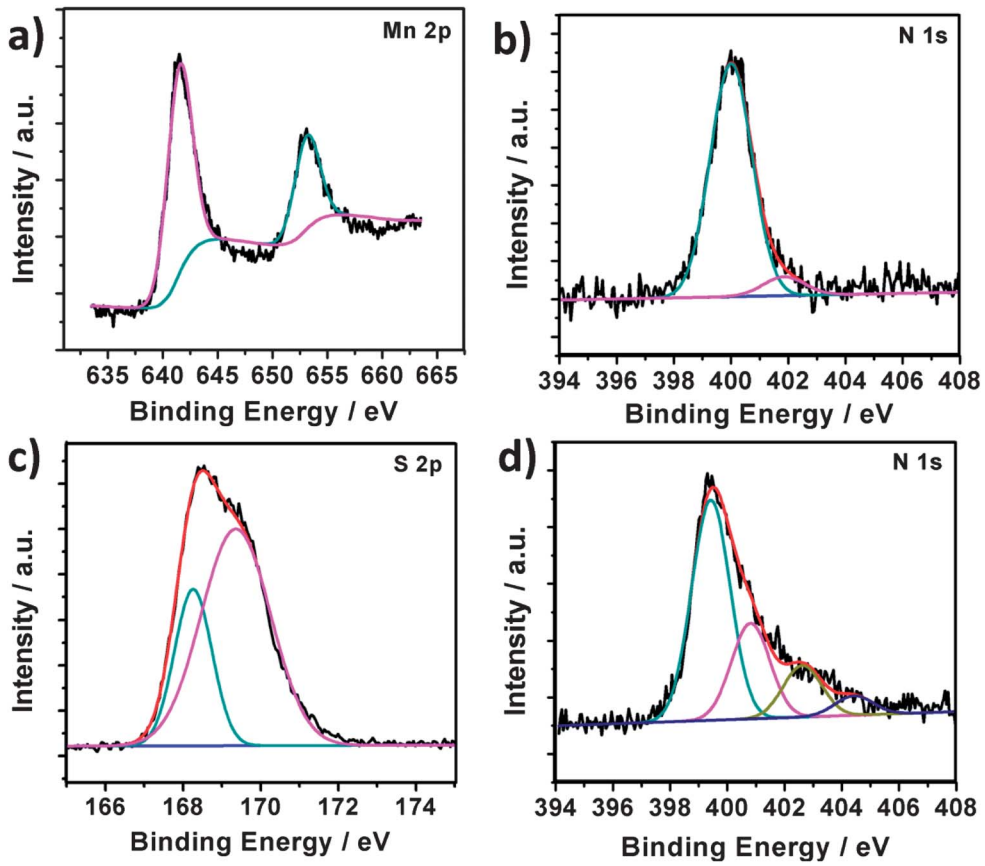

Fig. 3 (a) Mn 2p, (b) N 1s and (c) S 2p XPS core level spectra of PVP and SDS modified MnO_2; (d) N 1s XPS core level spectra of MnO_2/PANI coaxial NW.

Mn $2p_{3/2}$ and Mn $2p_{1/2}$ which are centered at 642 and 653.9 eV are in good agreement with reported data of Mn $2p_{3/2}$ and Mn $2p_{1/2}$ in MnO_2 NW (Fig. 3a). Further quantitative analysis through ICP-MS also supports the attainment of MnO_2 after polymerization of PANI. The weight percentage of MnO_2 is estimated to be around 25 wt% of the final MnO_2/PANI product.

The typical cyclic voltammogram of MnO_2 shows rectangular shape indicating the capacitive behavior of MnO_2 due to the fast, reversible, successive surface redox reactions of MnO_2.[1] However, common characteristic for most of the cyclic voltammogram of MnO_2 is that as the scan rate increases, the deviation from the rectangular-shaped curve became very obvious, especially at high scan rates. This is attributed to the slow diffusion of Na^+ and high resistivity of MnO_2 which lead to the distortion of the current response at the switching potential, poor rate capability and low specific capacitance. Electrochemical tests of MnO_2 NW, PANI and MnO_2/PANI coaxial NW were first studied by cyclic voltammetry (CV) between 0 and 0.9 V in 1 M Na_2SO_4. Cyclic voltammograms of each sample at scan rates of 10 and 100 mV s^{-1} are shown in Fig. 4a and b. Unlike the slightly distorted CV curve of PANI, the rectangular voltammetric responses at 10 mV s^{-1} of both MnO_2 NW and MnO_2/PANI coaxial NW samples indicate the ideal capacitive nature.[24,40] The wider area under the CV curve of MnO_2/PANI coaxial NW as compared to the other two samples shows the capacitive improvement after PANI coating. The difference in the area under the CV curve becomes more prominent at the scan rate of 100 mV s^{-1}, indicating better capacitive performance of MnO_2/PANI coaxial NW as compared to the other two samples at higher scan rate. Besides CVs, galvanic charge and discharge measurements were also carried out on all samples at different applied current ranging from 2 to 30 A g^{-1}. The resultant graph shows a straight line and symmetric charge and discharge curves (Fig. 4c).

The C_{sp} of each sample is calculated from its discharge curve. C_{sp} of PANI at 2 A g^{-1} is about 324 F g^{-1}. The calculated C_{sp} of MnO_2 NW at 2 A g^{-1} is about 377 F g^{-1}, which is relatively higher as compared to other α MnO_2 synthesized through hydrothermal treatment.[4,7] This improvement is because of the well dispersed nature of our nanowires which allows the electrolyte ions to reach all the active materials. The C_{sp} improves significantly after coating a layer of PANI. The calculated C_{sp} of MnO_2/PANI coaxial NW at 2 A g^{-1} (498 F g^{-1}) is higher than MnO_2 NW which indicates the contribution of the pseudocapacitance effect of PANI coated on the MnO_2 NW. We have also measured the performance at lower applied current: 0.25, 0.5, and 1 A g^{-1}, the resultant C_{sp} are much higher: 873, 663 and 574 F g^{-1}, respectively. The charge discharge curves of the samples at different applied currents are shown in Fig. 4c and ESI Fig. S3 and S4.† C_{sp} at other applied currents are also shown in Fig. 4d.

The electrochemical stability of each sample was examined under continuous cyclic voltammetry at 25 mV s^{-1} for 5000 cycles in 1 M Na_2SO_4 (Fig. 5a). The C_{sp} of MnO_2 NW was more

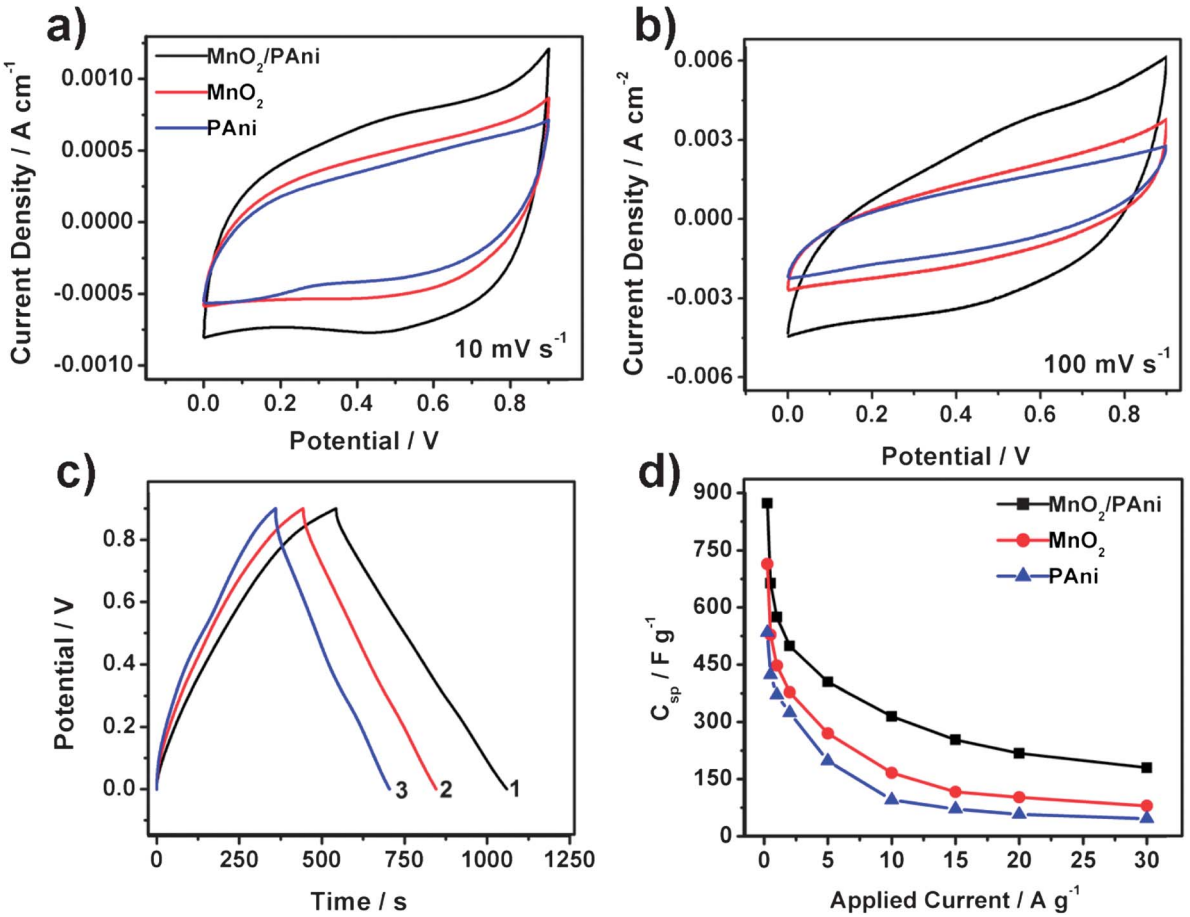

Fig. 4 (a and b) Cyclic voltammograms of MnO_2/PANI coaxial NW, MnO_2 NW and PANI at 10 and 100 mV s^{-1}. (c) Charge and discharge curve of MnO_2/PANI coaxial NW (1), MnO_2 NW (2) and PANI (3) at 2 A g^{-1}. (d) C_{sp} of MnO_2/PANI coaxial NW, MnO_2 NW and PANI measured at different applied current.

or less stable for up to 1000 cycles with 1% degradation of C_{sp}, indicating good stability of the sample. By the end of 3000 cycles, the capacitance loss was about 9% of its original C_{sp}. However, it continued to degrade significantly all the way until 5000 cycles (18% degradation). The cycling performance of PANI was the worst among the three samples. C_{sp} of PANI faded significantly during the first 100 cycles (11% degradation) and continued to degrade down to 30% at the end of 5000 cycles. It is well known that conducting polymers are prone to capacitive fading during the cycling test due to the continuous swelling and shrinkage of the polymer's structure. On the other hand, the C_{sp} of MnO_2/PANI coaxial NW was slightly reduced during the first 500 cycles, before it starts to stabilize. By the end of 5000 cycles, it retained about 95% of its original C_{sp}. The C_{sp} degradation of MnO_2 over the long term cycling test is often associated with the dissolution of MnO_2 into Mn^{2+} ions in the aqueous electrolyte.[47] From thermodynamic point of view, the Pourbaix diagram of the Mn–H_2O system suggests that some of the MnO_2 will eventually dissolve in Na_2SO_4.[48] This process reduces the amount of the active materials, thus slowly decreasing the C_{sp} of MnO_2 during the long cycling test. Coating a protection layer on MnO_2 has shown to improve the long term cycling stability of MnO_2.[26]

The performance of MnO_2/PANI coaxial NW reported in this work is superior as compared to other MnO_2/PANI and redox heterostructured nanomaterials powder based composites reported in the literature so far.[18,19,25–27,29,40] The improved specific capacitance, rate capability as well as cycling stability of MnO_2/PANI coaxial NW in this work can be attributed to the following reasons. First, by introducing a layer of conducting polymer, the ionic resistance within MnO_2 NW networks is reduced which can be seen from EIS measurement in Fig. 5b. At high frequency range, the intercept on Z real or X axis is related to the solution or ionic resistance (R_{sol}) while the diameter of the semicircle arc is related to the charge transfer resistance (R_{ct}).[11,49] The intercept at Z real axis of MnO_2 NW reduced from 5 to 2 Ω after coating a layer of conducting polymer PANI. In addition to the uniform PANI coating that is electrostatically bonded to the MnO_2 NW, the well maintained dispersed coaxial nanowire network structure helps the ions to reach most of the active materials. This configuration results in the lower charge transfer resistance at the interface of active materials and electrolyte which can be seen from the smaller diameter of the semicircle arc in the Nyquist plot of MnO_2/PANI coaxial NW as compared to MnO_2 NW.[49,50] Second, PANI provides additional redox reaction which can be seen from the enlarged area under the CV curve upon coating of PANI on the MnO_2 NW. PANI coating also acts as a protection layer to prevent the MnO_2 dissolution during the long cycling process which has been one of the major

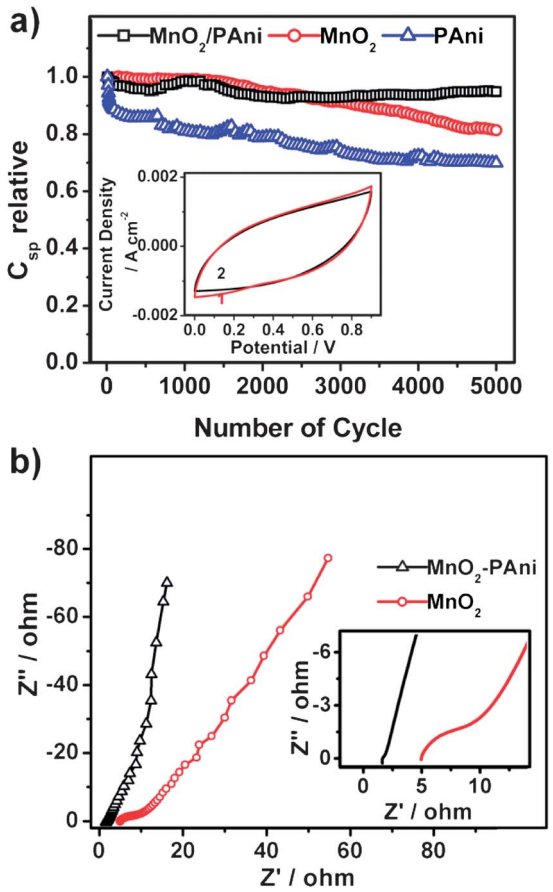

Fig. 5 (a) Relative C_{sp} during the extended cyclic voltammetry test at 25 mV s^{-1}, inset shows the cyclic voltammogram of MnO_2/PANI coaxial NW after 10^{th} cycle (1) and 5000^{th} cycle (2). (b) Nyquist plots of MnO_2/PANI coaxial NW and MnO_2 NW.

cause in the capacitive fading of MnO_2 during the long and continuous cycling test.[8,26] Third, good interaction between PANI and transition metal oxides improves the capacitive properties of this composite structure.[19] As discussed previously, the interaction between PANI and MnO_2 in our system can be enhanced through the presence of electrostatically bonded double surfactant layers which will enhance the charge transfer within the active materials. Fourth, the outstanding performance of this MnO_2/PANI coaxial NW is also due to the design geometry of the active materials. Instead of random location of PANI within the composite electrode, the polymerization process of PANI is self-terminated on the MnO_2 NW surface and resulted in the thin layer of PANI coating on the well dispersed MnO_2 NW. Chen *et al.* have used a linker molecule to graft PANI onto the surface of MnO_2 particles. C_{sp} as high as 415 F g^{-1} at 1.67 mA cm^{-2} has been achieved with 15% degradation after 1000 cycles.[19] This low performance is probably because of the difficulties in controlling the polymerization process of PANI which results in non-uniform distribution of PANI in the composite structure. On the contrary, our samples are able to maintain the well dispersed nanowires structure even after the coating of PANI. Lastly, this double surfactant method is versatile and can be extended to synthesize other transition metal oxides and PANI composites. In addition to the good performance of this material system, relatively low cost of MnO_2 and PANI is another advantage of this structure which is promising for its commercial application.

4. Conclusions

In summary, the enhanced interaction between redox active materials with the desirable heteronanostructures design could lead to the improvement of the capacitive performance of the composite materials. The MnO_2/PANI hybrid nanostructure reported in this work results in the improved conductivity, specific capacitance and cycling stability of the pseudocapacitor electrode. Higher C_{sp} has been achieved for MnO_2/PANI coaxial NW sample at all applied currents during the galvanic charge and discharge test (*e.g.* 498 F g^{-1} at 2 A g^{-1}) as compared to the pristine MnO_2 NW (377 F g^{-1}) and PANI (324 F g^{-1}). This work contributes significantly to the advancement in the synthetic approach of redox nanocomposites as well as fundamental understanding on improving the capacitance performance of redox heterostructure nanomaterials.

Acknowledgements

A. Sumboja acknowledges the scholarship awarded by NTU. This work is supported by Singapore National Research Foundation under CREATE programme Nanomaterials for Water and Energy Management.

Notes and references

1 P. Simon and Y. Gogotsi, *Nat. Mater.*, 2008, **7**, 845–854.
2 P. J. Hall, M. Mirzaeian, S. I. Fletcher, F. B. Sillars, A. J. R. Rennie, G. O. Shitta-Bey, G. Wilson, A. Cruden and R. Carter, *Energy Environ. Sci.*, 2010, **3**, 1238–1251.
3 Q. Qu, P. Zhang, B. Wang, Y. Chen, S. Tian, Y. Wu and R. Holze, *J. Phys. Chem. C*, 2009, **113**, 14020–14027.
4 V. Subramanian, H. Zhu, R. Vajtai, P. M. Ajayan and B. Wei, *J. Phys. Chem. B*, 2005, **109**, 20207–20214.
5 C. Yu, L. Zhang, J. Shi, J. Zhao, J. Gao and D. Yan, *Adv. Funct. Mater.*, 2008, **18**, 1544–1554.
6 D. Liu, B. B. Garcia, Q. Zhang, Q. Guo, Y. Zhang, S. Sepehri and G. Cao, *Adv. Funct. Mater.*, 2009, **19**, 1015–1023.
7 M. Xu, L. Kong, W. Zhou and H. Li, *J. Phys. Chem. C*, 2007, **111**, 19141–19147.
8 J. Yan, E. Khoo, A. Sumboja and P. S. Lee, *ACS Nano*, 2010, **4**, 4247–4255.
9 A. Sumboja, U. M. Tefashe, G. Wittstock and P. S. Lee, *J. Power Sources*, 2012, **207**, 205–211.
10 C. J. Xu, F. Y. Kang, B. H. Li and H. D. Du, *J. Mater. Res.*, 2010, **25**, 1421–1432.
11 H. L. Li, J. X. Wang, Q. X. Chu, Z. Wang, F. B. Zhang and S. C. Wang, *J. Power Sources*, 2009, **190**, 578–586.
12 G. A. Snook, P. Kao and A. S. Best, *J. Power Sources*, 2010, **196**, 1–12.
13 L. L. Zhang, S. Li, J. T. Zhang, P. Z. Guo, J. T. Zheng and X. S. Zhao, *Chem. Mater.*, 2010, **22**, 1195–1202.
14 A. Sumboja, X. Wang, J. Yan and P. S. Lee, *Electrochim. Acta*, 2012, **65**, 190–195.
15 C. Liu, F. Li, L. P. Ma and H. M. Cheng, *Adv. Mater.*, 2010, **22**, E28–E62.
16 R. Liu, J. Duay and S. B. Lee, *Chem. Commun.*, 2011, **47**, 1384–1404.
17 R. Liu, J. Duay and S. B. Lee, *ACS Nano*, 2010, **4**, 4299–4307.
18 J. Zang and X. Li, *J. Mater. Chem.*, 2011, **21**, 10965–10969.
19 L. Chen, L. J. Sun, F. Luan, Y. Liang, Y. Li and X. X. Liu, *J. Power Sources*, 2010, **195**, 3742–3747.
20 W. Y. Zou, W. Wang, B. L. He, M. L. Sun and Y. S. Yin, *J. Power Sources*, 2010, **195**, 7489–7493.

21 L. J. Sun, X. X. Liu, K. K. T. Lau, L. Chen and W. M. Gu, *Electrochim. Acta*, 2008, **53**, 3036–3042.
22 F. J. Liu, *J. Power Sources*, 2008, **182**, 383–388.
23 L. J. Sun and X. X. Liu, *Eur. Polym. J.*, 2008, **44**, 219–224.
24 W. Ni, D. Wang, Z. Huang, J. Zhao and G. Cui, *Mater. Chem. Phys.*, 2010, **124**, 1151–1154.
25 Z. Zhou, N. Cai and Y. Zhou, *Mater. Chem. Phys.*, 2005, **94**, 371–375.
26 C. Yuan, L. Su, B. Gao and X. Zhang, *Electrochim. Acta*, 2008, **53**, 7039–7047.
27 Q. Li, J. Liu, J. Zou, A. Chunder, Y. Chen and L. Zhai, *J. Power Sources*, 2011, **196**, 565–572.
28 Jaidev, R. I. Jafri, A. K. Mishra and S. Ramaprabhu, *J. Mater. Chem.*, 2011, **21**, 17601–17605.
29 X. F. Yang, G. C. Wang, R. Y. Wang and X. W. Li, *Electrochim. Acta*, 2010, **55**, 5414–5419.
30 K. R. Prasad and N. Miura, *Electrochem. Solid-State Lett.*, 2004, **7**, A425–A428.
31 R. Liu and S. B. Lee, *J. Am. Chem. Soc.*, 2008, **130**, 2942–2943.
32 C. L. Zhu, S. W. Chou, S. F. He, W. N. Liao and C. C. Chen, *Nanotechnology*, 2007, **18**, 275604–275610.
33 Y. Yang, G. Yu, J. J. Cha, H. Wu, M. Vosgueritchian, Y. Yao, Z. Bao and Y. Cui, *ACS Nano*, 2011, **5**, 9187–9193.
34 J. Wang, E. Khoo, J. Ma and P. S. Lee, *Chem. Commun.*, 2010, **46**, 2468–2470.
35 S. Devaraj and N. Munichandraiah, *J. Phys. Chem. C*, 2008, **112**, 4406–4417.
36 K. S. Ryu, S. K. Jeong, J. Joo and K. M. Kim, *J. Phys. Chem. B*, 2007, **111**, 731–739.
37 A. H. Gemeay, I. A. Mansour, R. G. El-Sharkawy and A. B. Zaki, *Eur. Polym. J.*, 2005, **41**, 2575–2583.
38 L. J. Pan, L. Pu, Y. Shi, S. Y. Song, Z. Xu, R. Zhang and Y. D. Zheng, *Adv. Mater.*, 2007, **19**, 461.
39 Z. Zhang, Z. Wei and M. Wan, *Macromolecules*, 2002, **35**, 5937–5942.
40 X. Zhang, L. Y. Ji, S. C. Zhang and W. S. Yang, *J. Power Sources*, 2007, **173**, 1017–1023.
41 G. Song, J. Han and R. Guo, *Synth. Met.*, 2007, **157**, 170–175.
42 S. Xiong, S. L. Phua, B. S. Dunn, J. Ma and X. Lu, *Chem. Mater.*, 2009, **22**, 255–260.
43 B. Sun, B. Duan and X. Yuan, *J. Appl. Polym. Sci.*, 2006, **102**, 39–45.
44 K. Takahashi and K. Nagai, *Polymer*, 1996, **37**, 1257–1266.
45 J. L. Duvail, P. Retho, V. Fernandez, G. Louarn, P. Molinie and O. Chauvet, *J. Phys. Chem. B*, 2004, **108**, 18552–18556.
46 X. R. Zeng and T. M. Ko, *Polymer*, 1998, **39**, 1187–1195.
47 W. F. Wei, X. W. Cui, W. X. Chen and D. G. Ivey, *Electrochim. Acta*, 2009, **54**, 2271–2275.
48 M. Pourbaix, *Atlas of Electrochemical Equilibria in Aqueous Solutions*, NACE International, Houston, 1974.
49 S. Devaraj and N. Munichandraiah, *J. Electrochem. Soc.*, 2007, **154**, A80–A88.
50 W. Xiao, H. Xia, J. Y. H. Fuh and L. Lu, *J. Electrochem. Soc.*, 2009, **156**, A627–A633.

